Cheng, K., Elrick, M., and Romaniello, S.J., 2020, Early Mississippian ocean anoxia triggered organic carbon burial and late Paleozoic cooling: Evidence from uranium isotopes recorded in marine limestone: Geology, v. 48, https://doi.org/10.1130/G46950.1

# Early Mississippian ocean anoxia triggered organic carbon burial and late Paleozoic cooling: evidence from uranium isotopes of marine limestones

## DATA REPOSITORY

## GEOLOGIC BACKGROUND

During the Early Mississippian, North American straddled the paleoequator and the Nevada study area lay in the paleotropics (Fig. 1A). Convergence of western North America with a volcanic arc during the Late Devonian to Early Mississippian led to the formation of the Antler foreland basin extending from Nevada to Canada where >500 m of Lower Mississippian deep- through shallow-marine and non-marine siliciclastics and carbonate deposits accumulated (Giles and Dickinson, 1995). The targeted Lower Mississippian limestone succession represents deposition in the eastern, carbonate-dominated portion of the Antler foreland basin during active convergent-margin tectonics.

The Early Mississippian spans the climatic transition between the Devonian greenhouse and late Carboniferous icehouse (late Paleozoic ice age or LPIA; Isbell et al., 2003; Montañez and Poulson, 2013). The timing of the LPIA onset is debated with Gondwanan glaciation beginning as early as the Middle Devonian (Elrick and Witzke, 2014; McGhee, 2015), the Late Devonian (Famennian; Caputo et al. 2008, Isaacson et al., 2008), to the Early Mississippian (Tournaisian; Buggisch et al., 2008; Kammer and Matchen, 2008; Wallace and Elrick, 2014). Alternatively, a Middle to Late Mississippian (Visean-Serpukovian) LPIA onset is suggested by the age of glacial deposits in Australia and South America (González, 2001; Limarino et al., 2006; Fielding et al., 2008; Isbell et al., 2003; Gulbranson et al., 2010), glacio-eustatically generated cyclothems (Bishop et al., 2009; Waters and Condon, 2012), climatically controlled changes in Gondwanan floral communities (Iannauzzi and Pfefferkorn, 2002), and a positive excursion of $\delta^{13}C$ and $\delta^{18}O$ (Mii et al., 1999; Buggisch et al., 2008; Giles, 2012; Maharjan et al., 2018b).

## FIELD AND LABORATORY METHODS

The Lower Mississippian Joana Limestone and Limestone X were measured and described on a bed-by-bed basis in the Pahranaghat Range of southern Nevada (Figs. 1, 2). Facies and corresponding depositional environments were interpreted using lithology, grain size, sorting, sedimentary structures, skeletal and trace fossil content, bed geometries, and facies associations (Table DR1). Facies stacking patterns were utilized to identify eleven ~0.5 - 1 My-scale depositional sequences shown in Figure 2.

Samples (bulk rock and individual large skeletal grains) were collected every 2-4 m throughout the ~250 m-thick section. To evaluate the effects of isotopic differences between primary skeletal calcite (representing original or near-original seawater values) versus coeval bulk limestone matrix (representing a combination of original seawater and diagenetic carbonate phases), individual corals, brachiopods, and crinoids were sampled and compared to coeval bulk limestone matrix. Bulk limestone samples were chipped into small fragments that were free from secondary carbonate veins and weathering and were powdered with a Spex 8510 shatterbox in an alumina puck pulverizer. Skeletal fragments were drilled and the powder was collected for geochemical analyses.

For each sample, approximately 1.5 grams of sample powder containing ~ 200-1000 ng of U was digested using ~50 mL trace metal-free 1M $HNO_3$ (see White et al. 2018 for details and explanations of digestion process and acid strengths). The purpose of using this relatively strong acid is to release all the uranium in the bulk carbonate and prevent potential fractionation occurring during partial dissolution of various secondary carbonate phases (cements) and back absorption of U onto undissolved phases such as clay and other undissolved minerals. During early diagenesis, uranium hosted by primary carbonate could be released due to dissolution and recrystallization and incorporated into secondary carbonate cements and carbonate fluorapatite, or the liberated U could have been reduced to U(IV) in anoxic porewaters. Incomplete carbonate dissolution might result in equilibrium uranium isotopic fractionation

between the different phases and produce isotopic offsets. On the other hand, bulk carbonate measurements could yield coherent stratigraphic trends in ancient carbonates (Zhang et al., 2018). Therefore, it is necessary to use relatively strong acid to prevent inconsistent isotopic offset by the incomplete release of carbonate-hosted uranium.

Following dissolution, samples were immediately centrifuged to remove solid insoluble residues. Major, minor, and trace element concentrations were subsequently determined on an aliquot of the supernatant using a iCAP-Q quadrupole ICP-MS at Arizona State University (W.M. Keck Foundation Laboratory for Environmental Biogeochemistry) at an overall dilution of 2000 X (approximately 200 ug/mL Ca). The remaining sample solution was spiked using the IRMM-3636 $^{233}U$-$^{236}U$ double spike (Verbruggen et al., 2008) following a ratio of 8.8 ng of spike/500 ng U in each sample. Spiked samples were transferred to Teflon vials and treated with 32 wt% $H_2O_2$ and 15.6M $HNO_3$ three times on a hot plate for 2 hours to digest organic matter. After digestion, samples underwent column chemistry to isolate and collect U following the UTEVA resin method (Weyer et al., 2008). The collected U solution was treated with 0.2 ml 32 wt% $H_2O_2$ and 1 ml 3M $HNO_3$ twice to remove any organic matter contamination from the UTEVA resin. Before $\delta^{238}U$ analysis, a second automated column chemistry was used to remove traces of Na and Fe using the ESI PrepFast-MC system. Samples were loaded onto 1 mL of Eichrom DGA resin in 6M $HNO_3$ and the sample matrix was eluted with 10 mL of 6 $HNO_3$ before eluting the U with 10 mL of 0.05 M HCl. Dried samples were subsequently redissolved and were analyzed for U isotope on a Thermo Neptune MC-ICP-MS at Arizona State University equipped with an ESI Apex-Q desolvating nebulizer, Jet sample cone, and H skimmer cone. Samples and standards were analyzed at a concentration of 50 ppb, producing 25-35 volts of signal intensity. Double-spiked samples were bracketed and normalized to identically double-spiked aliquots of CRM-145 U and accompanied by repeated analyses of CRM-129a as a secondary standard. Uranium isotope data was reported as the

mean of duplicate analyses of each sample solution, with measurement uncertainty assigned based on the in-run precision of repeated analyses of the bracketing CRM-145 standard (2sd = 0.08 ‰, N = 190). An F-test comparing the difference between variance of repeated analyses of CRM-145 and the mean square of the error (MSE) of samples was insignificant (P-value = 0.40), indicating the precision of sample and standard analyses was statistically indistinguishable (2sd = 0.08 ‰). Under these conditions, CRM-129a standard yielded an average $\delta^{238}U$ value of -1.69 ± 0.09 ‰ (N = 12) which agrees with Chen et al. (2018a) and Zhang et al. (2018). An aliquot of the in-house modern coral powder standard (PB-0010) processed in parallel with samples yielded $\delta^{238}U$ = -0.38 ± 0.10 ‰ (N = 4) in agreement with previously published literature values (Romaniello et al., 2013; Tissot and Dauphas, 2015; Chen et al., 2018b).

Carbon and oxygen isotopes analysis was conducted following the Spotl and Vennemann (2003) method. About 0.5 mg of powdered sample was loaded into 12 mL borosilicate tubes, flushed with He, then reacted with $H_3PO_4$ at 50°C for 12 hours. The $CO_2$ gas converted from the carbonate sample was measured for $\delta^{13}C$ and $\delta^{18}O$ values using continuous flow Isotope Ratio Mass Spectrometry with a Gasbench device coupled to a Thermo Fisher Scientific Delta V Plus Isotope Mass Spectrometer at the University of New Mexico Center for Stable Isotopes. The results are reported using the delta notation, versus V-PDB. Reproducibility was better than 0.1‰ for both $\delta^{13}C$ and $\delta^{18}O$ based on repeats of a laboratory standard (Carrara Marble). The laboratory standards were calibrated versus NBS 19, for which the $\delta^{13}C$ is 1.95‰ and $\delta^{18}O$ is -2.2‰.

## DIFFERENCES BETWEEN $\delta^{238}U$ SIGNATURES IN LIMESTONES VERSUS SHALES

It is important to highlight the difference between using $\delta^{238}U$ signatures from carbonate versus siliciclastic deposits for seawater redox studies. Paleozoic limestones formed mainly by carbonate-secreting benthic organisms living in less than a few tens of meters of water depths and were transported offshore by gravity-flow, storm, and tidal currents to accumulate as fine detrital carbonate

92 particles. Once deposited, they were cemented directly on the seafloor and/or in shallow- through
93 deep-burial diagenetic environments. This history implies that even though the fine detrital carbonate
94 particles may have ultimately accumulated in a range of poor to well oxygenated deeper water
95 environments, their authigenic U component (minus any diagenetic cements) was originally derived
96 from well-oxygenated, shallow-water environments. In contrast, offshore siliciclastic (mudrocks or
97 shales) obtained their authigenic U component from bottom waters (or porewaters); therefore, their
98 $\delta^{238}U$ signature reflects local conditions that may not reflect global seawaters. Given the original
99 shallow-water source for Paleozoic carbonate deposits, the redox signature provided by the $\delta^{238}U$ may
100 not match those interpreted from their depositional environment redox characteristics shown on Figure
101 2 (shaded vertical bar).

102 The studied Lower Mississippian limestones include offshore through shallow carbonate ramp
103 deposits (Fig. 1B); the finer grained offshore deposits were sourced from well-oxygenated, shallow-
104 water environments originally located farther east in Utah and Arizona (Giles and Dickinson, 1995).
105 Given the original oxygenated source for the offshore deposits, the redox signature provided by the
106 $\delta^{238}U$ may or may not match those interpreted from their depositional redox characteristics that were
107 interpreted using grain size, bioturbation intensity, presence/absence of benthic skeletal fossils,
108 sedimentary structures, and relative organic matter content.

109 **STRATIGRAPHIC RESULTS**

110 We identify 4 main depositional facies within the studied section, which are described in Table
111 DR1 and are interpreted below and with depositional redox interpretations shown in Figure 2. The dark
112 lime mudstone facies is interpreted to represent deposition in moderately to poorly oxygenated waters
113 within offshore to lower shoreface environments along the outer ramp. The relative oxygen levels are
114 interpreted from the occurrence of sparse, fine benthic skeletal material (brachiopods, crinoids, tabulate

115 corals) and sparse bioturbation (including *Zoophycus* and *Chondrites* trace fossils), and dark color.
116 Offshore to lower shoreface conditions are interpreted from the preserved suspension laminations, fine
117 graded beds and lenses, and association with adjacent offshore to lower shoreface facies. A ~7 m
118 interval (between 80-87 m; Fig. 2) is characterized by very few benthic and trace fossils suggesting a
119 brief period of poorly oxygenated conditions (but enough oxygen to support limited animal life). The
120 wackestone-lime mudstone facies (wackstone-mudstone) is interpreted to represent deposition under
121 moderately to well oxygenated waters within lower shoreface environments of the outer to middle
122 ramp. These oxygenation conditions are based on abundance of benthic skeletal and trace fossils and
123 relatively dark color, while lower shoreface environments are interpreted from the common graded
124 beds/lenses, abraded skeletal fossils, and association with adjacent offshore facies. The skeletal
125 wackestone facies is interpreted to represent deposition under well-oxygenated waters within lower
126 shoreface environments of the middle ramp. These oxygenated conditions are based on the abundance
127 of benthic skeletal fossils and bioturbation, and the light gray color. The lower shoreface environments
128 are interpreted from the common graded beds, abraded grains and association with adjacent offshore-
129 lower shoreface facies. The crinoidal packstone facies is interpreted to represent deposition under fully
130 oxygenated waters within upper shoreface environments of the inner ramp. The oxygenated conditions
131 are interpreted from the abundance of large skeletal grains, paucity of fine matrix, abundant
132 bioturbation, and the light color. The upper shoreface environments are interpreted from grain-
133 supported textures, large grain size and abrasion, rare cross bedding, and association with adjacent
134 lower shoreface facies.

135 Eleven depositional sequences (~15-30 m thick) are recognized based on facies stacking patterns
136 (Fig. 2). Transgressive systems of tracts (TSTs) of the Joana Limestone sequences are characterized by
137 progressive upward deepening from crinoidal packstone to skeletal wackestone facies. Maximum

flooding zones (MFZs) are comprised of skeletal wackstone facies, and highstand systems tracts (HSTs) are typified by upward-shallowing successions of skeletal wackstone to crinoidal packstone facies. Sequences within Limestone X are characterized by TSTs composed of skeletal wackstone to lime mudstone facies, MFZs are composed of meter-thick intervals of lime mudstone/skeletal wackstone, and HSTs are characterized by skeletal wackstone overlain by crinoidal packstones. Sequence boundaries in both the Joana Limestone and Limestone X are defined at the top of the shallowest water facies immediately before abrupt deepening trends related to the overlying TST. No evidence of subaerial exposure is observed in the field (i.e., karsting, brecciation, paleosols) indicating relatively continuous deposition throughout the duration of the studied succession.

## EVALUATING LOCAL VS GLOBAL $\delta^{238}U$ SIGNATURES

*Authigenic U component*

We estimate the fraction of authigenic U in samples to evaluate whether the measured $\delta^{238}U$ values are derived from authigenic versus detrital phases using the U enrichment factor (UEF) defined as:

$$UEF = (U_{sample}/Al_{sample}) / (U_{PAAS}/Al_{PAAS})$$

where UEF is the U enrichment factor of samples, $U_{sample}$ and $Al_{sample}$ are U and Al concentrations, and $U_{PAAS}$ and $Al_{PAAS}$ are U and Al concentrations of post-Archaean average shale (McLennan, 2001). UEF values of >1 represent higher enrichment in uranium relative to shale (i.e., higher than average detrital U values; Morford and Emerson, 1999; Piper and Perkins, 2004; Tribovillard et al., 2006). Early Mississippian UEFs range from 21 to 1182 (average = 438; Fig. DR2) which is significantly >1 and supports the hypothesis that most of the measured U is authigenic rather than detrital.

*Diagenesis*

To evaluate the effects of diagenesis on $\delta^{238}U$ values, we separately sampled primary skeletal grains (brachiopods, rugose coral, crinoids) versus coeval bulk limestone matrix. Results indicate the skeletal grains and bulk are within error of each other (Table DR4). These results differ from those reported in earlier studies wherein bulk matrix values were isotopically enriched compared to their coeval skeletal grains (Bartlett et al., 2018; White et al., 2018). These Mississippian results suggest that either the secondary cements in the bulk matrix were precipitated in well-oxygenated porewaters in communication with the overlying seawater, or that skeletal grains were isotopically enriched during diagenesis similar to that of the bulk matrix. The latter scenario implies that isotopic enrichment of skeletal grains occurred during 1) the transition and stabilization from high- to low-Mg calcite in crinoids, 2) recrystallization of original low-Mg calcite in brachiopods, or 3) that intra-skeletal cements precipitated from reducing porewaters contaminated the sample during drilling of individual samples. Further petrographic studies are required to differentiated between these possibilities.

***MODELING***

*U modeling – Initial Conditions*

To better quantify the influence of anoxia on seawater $\delta^{238}U$ values, we assume that the pre-Tournaisian OAE oceanic uranium cycle was in steady state. The $\delta^{238}U$ profile corrected for diagenetic offsets shows a significantly lower Early Mississippian seawater background value (~0.68‰) than today (-~0.39‰; Tissot and Dauphas, 2015), implying that the steady state U concentration in Early Mississippian ocean was different from today. Therefore, we use a steady state mass balance model (Montoya-Pino et al. 2010) to constrain the initial Early Mississippian U seawater conditions. The steady state mass balance equation for the seawater U inventory and its isotopic composition is:

$$\delta^{238}U_{river} = f_{eux\ flux} \times \delta^{238}U_{eux} + (1 - f_{eux\ flux}) \times \delta^{238}U_{oxic} \quad (1)$$

$$\delta^{238}U_{eux} = \delta^{238}U_{seawater} + \Delta_{eux} \quad (2)$$

$$\delta^{238}U_{oxic} = \delta^{238}U_{seawater} + \Delta_{oxic} \quad (3)$$

where $\delta^{238}U_{seawater}$, $\delta^{238}U_{eux}$ and $\delta^{238}U_{oxic}$ are U isotopic compositions of seawater, euxinic and oxic sedimentary sinks, respectively. The cap delta notation (Δ) is used to express U fractionation between seawater and sediment. The $f_{eux\ flux}$ represents the fraction of euxinic sequestration of U, which can also be expressed as a function of sediment area ($A_{eux}$ and $A_{oxic}$) and U concentration in the ocean ($N_u/V_{ocean}$):

$$f_{eux\ flux} = J_{eux}/(J_{eux} + J_{oxic}) \quad (4)$$

$$J_{oxic} = k_{oxic} \times A_{oxic} \times N_u/V_{ocean} \quad (5)$$

$$J_{eux} = k_{eux} \times A_{eux} \times N_u/V_{ocean} = k_{eux} \times A_{ocean} \times f_{eux} \times N_u/V_{ocean} \quad (6)$$

where k values are modern measured uranium burial rates and $N_u$ is the U oceanic reservoir size (Table DR2). Combining equations 1-6, we solve for the euxinic seafloor percentage ($f_{eux}$) and the oceanic reservoir ($N_u$) in steady state:

$$f_{eux} = \frac{\frac{\delta^{238}U_{river} - \delta^{238}U_{seawater} - \Delta_{oxic} \times k_{oxic}}{\Delta_{eux} - \Delta_{oxic}}}{k_{eux} - \frac{\delta^{238}U_{river} - \delta^{238}U_{seawater} - \Delta_{oxic} \times (k_{oxic} - k_{eux})}{\Delta_{eux} - \Delta_{oxic}}} \quad (7)$$

$$N_u = J_{riv}/(k_{eux} \times A_{ocean} \times f_{eux} + k_{oxic} \times A_{ocean} \times (1\text{-}f_{eux})) \quad (8)$$

With the initial steady state determined, we calculate changes in the euxinic seafloor percentage ($f_{eux}$), euxinic U flux ($f_{eux\ flux}$), and U oceanic reservoir size ($N_u$) using the dynamic model described below.

*U modeling –Dynamic Modeling*

To quantitatively estimate the change in euxinic seafloor area and the flux of seawater U to sediment sinks during the Tournaisian OAE, we use a modified model of Lau et al. (2016) and include oxic and euxinic sediment sinks. The mass balance equation for the seawater U inventory and its isotopic composition is:

$$dN_u/dt = J_{river} - J_{eux} - J_{oxic} \quad (9)$$

$$N_u \times d\delta^{238}U_{seawater}/dt = J_{river} \times (\delta^{238}U_{river} - \delta^{238}U_{seawater}) - J_{eu} \times \Delta_{eux} - J_{oxic} \times \Delta_{oxic} \quad (10)$$

where J values are U source and sink fluxes, respectively, introduced by river ($J_{river}$) and sequestered in euxinic ($J_{eux}$) and oxic ($J_{oxic}$) sediments. Combining equations 2-6 and 9-10, the euxinic seafloor fraction ($f_{eux}$) can be expressed by:

$$f_{eux} = (J_{river} \times (\delta^{238}U_{river} - \delta^{238}U_{seawater}) - N_u \times d\delta^{238}U_{seawater}/dt) / (k_{eux} \times A_{ocean} \times N_u/V_{ocean}) \times \Delta_{eux} \quad (11)$$

The uranium euxinic flux fraction ($f_{eux\ flux}$) can be expressed by:

$$F_{eux\ flux} = J_{eux} / J_{total} = J_{eux} / (J_{oxic} + J_{eux}) = (k_{eux} \times A_{ocean} \times f_{eux} \times N_u/V_{ocean}) / (k_{eux} \times A_{ocean} \times f_{eux} \times N_u/V_{ocean} + k_{oxic} \times A_{ocean} \times (1-f_{eux}) \times N_u/V_{ocean}) \quad (12)$$

Previous studies reported the effects of the diagenetic addition of isotopically heavy $\delta^{238}U$ from oxygen-depleted porewaters upon burial (Romaniello et al., 2013; Chen et al., 2018a). To correct for this diagenetic offset in this model, we subtract the value of 0.27‰ (Chen et al., 2018a) from our LOWESS-smoothed $\delta^{238}U$ curve.

Results of our dynamic U model calculations are shown in Figure 4 and suggest that ~30% of the global seafloor experienced euxinic conditions and up to 90% of the seawater U fluxed to euxinic sediments (leaving seawater significantly reduce in U concentration) during the Tournaisian OAE peak.

This model utilizing euxinic and oxic sediment sinks fails, however, to explain continued OC burial indicated by the second TICE peak because the area of euxinic seafloor returns to ~5% background values resulting in little/no OC burial and elevated $\delta^{13}C$ values. To better reproduce the observed double TICE peak, we modify the dynamic model to include three sediment sinks (oxic, anoxic/suboxic, euxinic and their respective U fractionation) using the following equation:

$$N_u \times d\delta^{238}U_{seawater}/dt = J_{river} \times (\delta^{238}U_{river} - \delta^{238}U_{seawater}) - J_{eux} \times \Delta_{eux} - J_{anox} \times \Delta_{anox} - J_{oxic} \times \Delta_{oxic} \quad (13)$$

where $J_{anox}$ and $\Delta_{anox}$ represent U flux into anoxic/suboxic sinks and its associated lower U fractionation (0.2‰, Morford and Emerson, 1999; Andersen et al., 2016). To simplify the modeling, we introduce the term R, which is the fraction of anoxic/suboxic seafloor ($f_{anoxic}$) divided by the fraction of total seafloor experiencing anoxic/suboxic and euxinic conditions:

$$R = f_{anox} / (f_{anox} + f_{eux}) \quad (14)$$

Note that this R definition is not the same as the percentage seafloor experiencing anoxic/suboxic or euxinic conditions that is shown in Figure 4G.

Our best-fit (though non-unique) model curve was generated using the following conditions: from 0 ky to 1280 ky (peak OAE), the area of euxinic seafloor was increased from ~5% to ~30% (R= 0; with no anoxic/suboxic seafloor). From 1280 ky to 1800 ky, the area of euxinic seafloor was decreased while the area of anoxic/suboxic seafloor was increased (R increases to 60%), which resulted in continued though decreasing OC burial and decreased U sequestration and fractionation (resulting in increased $\delta^{238}U$ values terminating the Tournaisian OAE). Between 1800 ky and 2200 ky, both euxinic and anoxic/suboxic seafloor areas were increased (resulting in increased OC burial and increased $\delta^{13}C$ values forming the second TICE peak, but with limited U fractionation) with the area of anoxic/suboxic

seafloor occupying approximately two-thirds of the total area of oxygen-depleted seafloor (R = constant at 60%). From 2200 ky to 2500 ky, the area of anoxic/suboxic and euxinic seafloor was decreased slightly, but with anoxic/suboxic conditions still dominating (R increases to 65%). Between 2500 ky and 4000 ky, the area of anoxic/suboxic and euxinic seafloor was gradually decreased to generate decreasing $\delta^{13}C$ values and the slight increase in measured $\delta^{238}U$ trends (R = constant at 65%).

*Carbon burial modeling*

Organic carbon burial estimates (using Kump and Arthur, 1999 model) from the observed $\delta^{13}C$ curve start by expressing the seawater carbonate isotopic composition as:

$$d\delta_{carb}/dt = (F_w \times (\delta_w - \delta_{carb}) - F_{bcarb} \times \Delta_{carb} - F_{borg} \times (\Delta_{org}))/M$$

where $\delta_{carb}$ and M are the isotopic composition and atmospheric and marine dissolved inorganic carbon (DIC) reservoir size (assumed in steady state), respectively. Volcanism-metamorphism and weathering of carbonate rocks and organic matter are the major carbon sources into the atmosphere-oceanic reservoir ($F_w$) and their average isotopic composition can be expressed as ($\delta_w$). The burial of carbonate C ($F_{bcarb}$) and organic C ($F_{borg}$) into sediments is a major sink of carbon. $\Delta_{carb}$ and $\Delta_{org}$ are the isotopic differences between DIC-calcite and DIC-organic matter, respectively. To simplify the calculation, we assume there is no fractionation during calcite precipitation ($\Delta_{carb}$= 0). The organic carbon burial flux derived from carbonate $\delta^{13}C$ curve can be expressed by:

$$F_{borg} = F_w \times (\delta_w - \delta_{carb}) - M \times d\delta_{carb}/dt$$

Results from the C modeling are shown in Figure 4F which shows two OC burial peaks that correspond well to the observed double peak TICE. When these results are combined with the U modeling described above, we interpret that the first OC burial peak was due to expanded euxinic seafloor conditions and the second peak was due mostly to expanded anoxic/suboxic seafloor conditions.

## CARBON MODELING OF THE LATE ORDOVICIAN (HIRNANTIAN) OR HICE EVENT

We estimate OC burial amounts for the Late Ordovician (Hirnantian) positive $\delta^{13}C$ excursion (HICE) using the same C model described above for the TICE. For the modeling, we assumed a HICE duration of between ~300 ky (estimated from White et al. 2018) to 1 My (estimated using the approximate duration of the Hirnantian stage) and using a range of HICE magnitudes of between 4‰ (Anticosti Island; Ghienne et al., 2013) and 7‰ (Copenhagen Canyon, Nevada; Kump et al., 1999).

## REFERENCES


Andersen, M., Vance, D., Morford, J., Bura-Nakić, E., Breitenbach, S., and Och, L., 2016, Closing in on the marine $^{238}U/^{235}U$ budget: Chemical Geology, v. 420, p. 11–22, doi: 10.1016/j.chemgeo.2015.10.041.

Bartlett, R., Elrick, M., Wheeley, J.R., Polyak, V., Desrochers, A., and Asmerom, Y., 2018, Abrupt global-ocean anoxia during the Late Ordovician–early Silurian detected using uranium isotopes of marine carbonates: Proceedings of the National Academy of Sciences, v. 115, p. 5896–5901, doi: 10.1073/pnas.1802438115.

Berner, R.A., and Raiswell, R., 1983, Burial of organic carbon and pyrite sulfur in sediments over phanerozoic time: a new theory: Geochimica et Cosmochimica Acta, v. 47, p. 855–862, doi: 10.1016/0016-7037(83)90151-5.

Caputo, M. V., de Melo, J. H. G., Streel, M., Isbell, J. L., & Fielding, C. R. (2008). Late Devonian and early Carboniferous glacial records of South America. *Geological Society of America Special Papers*, *441*, p. 161-173.

Bishop, J.W., Montañez, I.P., Gulbranson, E.L., and Brenckle, P.L., 2009, The onset of mid-Carboniferous glacio-eustasy: Sedimentologic and diagenetic constraints, Arrow Canyon, Nevada: Palaeogeography, Palaeoclimatology, Palaeoecology, v. 276, p. 217–243, doi: 10.1016/j.palaeo.2009.02.019.

Blakey, R.C., 2016. Colorado Plateau Geosystems: https://deeptimemaps.com/wp-content/uploads/2016/05/340_Ma_Miss_GPT-1.png (accessed May 2019)

Buggisch, W., Joachimski, M.M., Sevastopulo, G., and Morrow, J.R., 2008, Mississippian δ13Ccarb and conodont apatite δ18O records — Their relation to the Late Palaeozoic Glaciation: Palaeogeography, Palaeoclimatology, Palaeoecology, v. 268, p. 273–292, doi: 10.1016/j.palaeo.2008.03.043.

Caputo, M.V., Melo, J.H.G.D., Streel, M., and Isbell, J.L., 2008, Late Devonian and Early Carboniferous glacial records of South America: Special Paper 441: Resolving the Late Paleozoic Ice Age in Time and Space, p. 161–173, doi: 10.1130/2008.2441(11).

Chen, X., Romaniello, S.J., Herrmann, A.D., Hardisty, D., Gill, B.C., and Anbar, A.D., 2018a, Diagenetic effects on uranium isotope fractionation in carbonate sediments from the Bahamas: Geochimica et Cosmochimica Acta, v. 237, p. 294–311, doi: 10.1016/j.gca.2018.06.026.

Chen X., Romaniello, S.J., Herrmann, A.D., Samankassou, E., Anbar, A.D., 2018b, Biological effects on uranium isotope fractionation ($^{238}U/^{235}U$) in primary biogenic carbonates. Geochimica et Cosmochimica Acta, v. 240, p. 1-10, doi: 10.1016/j.gca.2018.08.028.

Dunk, R., Mills, R., and Jenkins, W., 2002, A reevaluation of the oceanic uranium budget for the Holocene: Chemical Geology, v. 190, p. 45–67, doi: 10.1016/s0009-2541(02)00110-9.

Fielding, C.R., Frank, T.D., Birgenheier, L.P., Rygel, M.C., Jones, A.T., and Roberts, J., 2008, Stratigraphic imprint of the Late Palaeozoic Ice Age in eastern Australia: a record of alternating glacial and nonglacial climate regime: Journal of the Geological Society, v. 165, p. 129–140.

Ghienne, J.-F., Desrochers, A., Vandenbroucke, T.R., Achab, A., Asselin, E., Dabard, M.-P., Farley, C., Loi, A., Paris, F., Wickson, S., and Veizer, J., 2014, A Cenozoic-style scenario for the end-Ordovician glaciation: Nature Communications, v. 5, doi: 10.1038/ncomms5485.

Giles, P.S., 2012, Low-latitude Ordovician to Triassic brachiopod habitat temperatures (BHTs) determined from $\delta^{18}O$[brachiopod calcite]: A cold hard look at ice-house tropical oceans: Palaeogeography, Palaeoclimatology, Palaeoecology, v. 317-318, p. 134–152, doi: 10.1016/j.palaeo.2012.01.002.

González, C.R. New data on the late Palaeozoic glaciations in Argentina: Newsletter on Carboniferous Stratigraphy, v. 19, p. 44–45.

Gulbranson, E.L., Montanez, I.P., Schmitz, M.D., Limarino, C.O., Isbell, J.L., Marenssi, S.A., and Crowley, J.L., 2010, High-precision U-Pb calibration of Carboniferous glaciation and climate history, Paganzo Group, NW Argentina: Geological Society of America Bulletin, v. 122, p. 1480–1498, doi: 10.1130/b30025.1.

Iannuzzi, R. and Pfefferkorn, H. W., 2002, A pre-glacial, warm-temperate floral belt in Gondwana (Late Visean, Early Carboniferous). Palaios, 17, v. 6, p. 571-590.

Isaacson, P., Díaz-Martínez, E., Grader, G., Kalvoda, J., Babek, O., and Devuyst, F., 2008, Late Devonian–earliest Mississippian glaciation in Gondwanaland and its biogeographic consequences: Palaeogeography, Palaeoclimatology, Palaeoecology, v. 268, p. 126–142, doi: 10.1016/j.palaeo.2008.03.047.

Isbell, J.L., Miller, M.F., Wolfe, K.L., and Lenaker, P.A., 2003, Timing of late Paleozoic glaciation in Gondwana: Was glaciation responsible for the development of Northern Hemisphere cyclothems?: Special Paper 370: Extreme depositional environments: mega end members in geologic time, p. 5–24, doi: 10.1130/0-8137-2370-1.5.

Johnson, J.G., Klapper, G., and Sandberg, C.A., 1985, Devonian eustatic fluctuations in Euramerica: Geological Society of America Bulletin, v. 96, p. 567, doi: 10.1130/0016-7606.

Kammer, T.W., and Matchen, D.L., 2008, Evidence for eustasy at the Kinderhookian-Osagean (Mississippian) boundary in the United States: Response to late Tournaisian glaciation: Special Paper 441: Resolving the Late Paleozoic Ice Age in Time and Space, p. 261–274, doi: 10.1130/2008.2441(18).

Kump, L. R. and Arthur, M. A., 1999, Interpreting carbon-isotope excursions: carbonates and organic matter, Chemical Geology, v. 161, p. 181-198.

Kump, L.R., Arthur, M.A., Patzkowsky, M.E., Gibbs, M.T., Pinkus, D.S., and Sheehan, P.M., 1999, A weathering hypothesis for glaciation at high atmospheric $pCO_2$ during the Late Ordovician: Palaeogeography, Palaeoclimatology, Palaeoecology, v. 152, p. 173–187, doi: 10.1016/s0031-0182(99)00046-2.

Kump, L.R., and Arthur, M.A., 1999, Interpreting carbon-isotope excursions: carbonates and organic matter: Chemical Geology, v. 161, p. 181–198, doi: 10.1016/s0009-2541(99)00086-8.

Lau, K.V., Maher, K., Altiner, D., Kelley, B.M., Kump, L.R., Lehrmann, D.J., Silva-Tamayo, J.C., Weaver, K.L., Yu, M., and Payne, J.L., 2016, Marine anoxia and delayed Earth system recovery after the end-Permian extinction: Proceedings of the National Academy of Sciences, v. 113, p. 2360–2365, doi: 10.1073/pnas.1515080113.

362 Limarino, C., Tripaldi, A., Marenssi, S., and Fauqué, L., 2006, Tectonic, sea-level, and climatic controls on
363 Late Paleozoic sedimentation in the western basins of Argentina: Journal of South American Earth
364 Sciences, v. 22, p. 205–226, doi: 10.1016/j.jsames.2006.09.009.

365 Lutgens, F.K., Tarbuck, E.J., and Tasa, D., 2018, Essentials of Geology: New York, Pearson, p 269.

366 Maharjan, D., Jiang, G., Peng, Y., and Henry, R.A., 2018a, Paired carbonate-organic carbon and nitrogen
367 isotope variations in Lower Mississippian strata of the southern Great Basin, western United States:
368 Palaeogeography, Palaeoclimatology, Palaeoecology, v. 490, p. 462–472, doi:
369 10.1016/j.palaeo.2017.11.026.

370 Maharjan, D., Jiang, G., Peng, Y., and Nicholl, M.J., 2018b, Sulfur isotope change across the Early
371 Mississippian K–O (Kinderhookian–Osagean) δ13C excursion: Earth and Planetary Science Letters, v. 494,
372 p. 202–215, doi: 10.1016/j.epsl.2018.04.043.

373 McManus, J., Berelson, W.M., Severmann, S., Poulson, R.L., Hammond, D.E., Klinkhammer, G.P., and
374 Holm, C., 2006, Molybdenum and uranium geochemistry in continental margin sediments: Paleoproxy
375 potential: Geochimica et Cosmochimica Acta, v. 70, p. 4643–4662, doi: 10.1016/j.gca.2006.06.1564.

376 Mclennan, S.M., 2001, Relationships between the trace element composition of sedimentary rocks and
377 upper continental crust: Geochemistry, Geophysics, Geosystems, v. 2, doi: 10.1029/2000gc000109.

378 Mii, H.-S., Grossman, E.L., and Yancey, T.E., 1999, Carboniferous isotope stratigraphies of North America:
379 Implications for Carboniferous paleoceanography and Mississippian glaciation: Geological Society of
380 America Bulletin, v. 111, p. 960–973, doi: 10.1130/0016-7606(1999)111<0960:cisona>2.3.co;2.

381 Montoya-Pino, C., Weyer, S., Anbar, A.D., Pross, J., Oschmann, W., Schootbrugge, B.V.D., and Arz, H.W.,
382 2010, Global enhancement of ocean anoxia during Oceanic Anoxic Event 2: A quantitative approach
383 using U isotopes: Geology, v. 38, p. 315–318, doi: 10.1130/g30652.1.

384 Montañez, I.P., and Poulsen, C.J., 2013, The Late Paleozoic Ice Age: An Evolving Paradigm: Annual
385 Review of Earth and Planetary Sciences, v. 41, p. 629–656.

386 Morford, J.L., and Emerson, S., 1999, The geochemistry of redox sensitive trace metals in sediments:
387 Geochimica et Cosmochimica Acta, v. 63, p. 1735–1750, doi: 10.1016/s0016-7037(99)00126-x.

388 Morford, J.L., Martin, W.R., and Carney, C.M., 2009, Uranium diagenesis in sediments underlying bottom
389 waters with high oxygen content: Geochimica et Cosmochimica Acta, v. 73, p. 2920–2937, doi:
390 10.1016/j.gca.2009.02.014.

391 Piper, D., and Perkins, R., 2004, A modern vs. Permian black shale—the hydrography, primary
392 productivity, and water-column chemistry of deposition: Chemical Geology, v. 206, p. 177–197, doi:
393 10.1016/j.chemgeo.2003.12.006.

394 Romaniello, S.J., Herrmann, A.D., and Anbar, A.D., 2013, Uranium concentrations and $^{238}U/^{235}U$ isotope
395 ratios in modern carbonates from the Bahamas: Assessing a novel paleoredox proxy: Chemical Geology,
396 v. 362, p. 305–316, doi: 10.1016/j.chemgeo.2013.10.002.

397 Spötl, C., and Vennemann, T.W., 2003, Continuous-flow isotope ratio mass spectrometric analysis of
398 carbonate minerals: Rapid Communications in Mass Spectrometry, v. 17, p. 1004–1006, doi:
399 10.1002/rcm.1010.

The World Ocean. The Columbia Encyclopedia. CD-ROM. 2007, 6th Ed. New York: Columbia University Press.

Tissot, F.L., and Dauphas, N., 2015, Uranium isotopic compositions of the crust and ocean: Age corrections, U budget and global extent of modern anoxia: Geochimica et Cosmochimica Acta, v. 167, p. 113–143, doi: 10.1016/j.gca.2015.06.034.

Tribovillard, N., Algeo, T.J., Lyons, T., and Riboulleau, A., 2006, Trace metals as paleoredox and paleoproductivity proxies: An update: Chemical Geology, v. 232, p. 12–32, doi: 10.1016/j.chemgeo.2006.02.012.

Verbruggen, A., Alonso, A., Eykens, R., Kehoe, F., Kuhn, H., Richter, S., and Aregbe, Y., 2008, Preparation and certification of IRMM-3636, IRMM-3636a and IRMM-3636b: JRC Scientific and Technical Reports, doi: 10.2787/60083.

Wallace, Z.A., and Elrick, M., 2014, Early Mississippian orbital-scale glacio-eustasy detected from high-resolution oxygen isotopes of marine apatite (conodonts): Journal of Sedimentary Research, v. 84, p. 816–824, doi: 10.2110/jsr.2014.69.

Waters, C.N., and Condon, D.J., 2012, Nature and timing of Late Mississippian to Mid-Pennsylvanian glacio-eustatic sea-level changes of the Pennine Basin, UK: Journal of the Geological Society, v. 169, p. 37–51, doi: 10.1144/0016-76492011-047.

White, D.A., Elrick, M., Romaniello, S., and Zhang, F., 2018, Global seawater redox trends during the Late Devonian mass extinction detected using U isotopes of marine limestones: Earth and Planetary Science Letters, v. 503, p. 68–77, doi: 10.1016/j.epsl.2018.09.020.

Zhang, F., Algeo, T.J., Romaniello, S.J., Cui, Y., Zhao, L., Chen, Z.-Q., and Anbar, A.D., 2018, Congruent Permian-Triassic $\delta^{238}U$ records at Panthalassic and Tethyan sites: Confirmation of global-oceanic anoxia and validation of the U-isotope paleoredox proxy: Geology, v. 46, p. 327–330, doi: 10.1130/g39695.1.

Zheng, Y., Anderson, R.F., Geen, A.V., and Kuwabara, J., 2000, Authigenic molybdenum formation in marine sediments: a link to pore water sulfide in the Santa Barbara Basin: Geochimica et Cosmochimica Acta, v. 64, p. 4165–4178, doi: 10.1016/s0016-7037(00)00495-6.

Zheng, Y., Anderson, R.F., Geen, A.V., and Fleisher, M.Q., 2002, Preservation of particulate non-lithogenic uranium in marine sediments: Geochimica et Cosmochimica Acta, v. 66, p. 3085–3092, doi: 10.1016/s0016-7037(01)00632-9.

**DR Figure captions**

**Figure DR1.** $\delta^{13}C$ and $\delta^{18}O$ (conodont apatite) trends from the Late Devonian to Late Mississippian from Buggisch et al. (2008). The gray shaded band outlines the Tournaisian OAE recognized in this study and the doubled-headed arrow outlines the Tournaisian carbon isotope excursion (TICE). Diagonal arrow on $\delta^{18}O$ curve outlines the positive shift that coincidences with the TICE onset indicating seawater cooling associated with widespread carbon burial.

**Figure DR2.** $\delta^{238}U$, $\delta^{13}C$, and $\delta^{18}O$, and selected elemental trends versus stratigraphic thickness.

**Table DR1.** Facies descriptions, depositional environments, and depositional oxygenation interpretations of Joana Limestone and Limestone X facies at the Pahranagat Range section, southern Nevada.

**Table DR2.** Parameters used in dynamic U modeling.

**Table DR3.** Parameters used in carbon burial modeling.

**Table DR4.** Data table showing sample numbers, meters, isotopic and elemental values, and sample lithology.

Penn.

Bashkir.

Namurian

Serpukh.

Conodont zonation

*Declinognathodus noduliferus*

*Gnathodus postbilineatus*

*Gnathodus b. bollandensis*

*Lochriea ziegleri*
*Lochriea cruciformis*

Mississippian

Viséan

326.5

*Lochriea multinodosa*

V3c

*Lochriea nodosa*

*Gnathodus bilineatus*

V3b

*Gnathodus praebilineatus*

*Gnathodus girtyi girtyi*

V3a

*Lochriea commutata*

V2b

V2a

*Lochriea cracoviensis*

V1b

*Gnathodus texanus*

V1b

*Gn. homopunctatus*

Tournaisian

346.7

*Scaliognathus anchoralis*

Tn3

*Gnathodus typicus*

S. isosticha - Lt. S. crenulata

Tn2

*E. Siphonodella crenulata*

*Siphonodella sandbergi*

Tn1b

*Siphonodella duplicata*

*Siphonodella sulcata*

Devonian

Famennian

358

*Siphonodella praesulcata*

*Palmatolepis expansa*

TICE

0 1 2 3 4 5 6

$\delta^{13}C_{carb}$ VPDB

18 19 20 21 22 23

$\delta^{18}O_{apatite}$ VSMOW

Ma

330

340

350

360

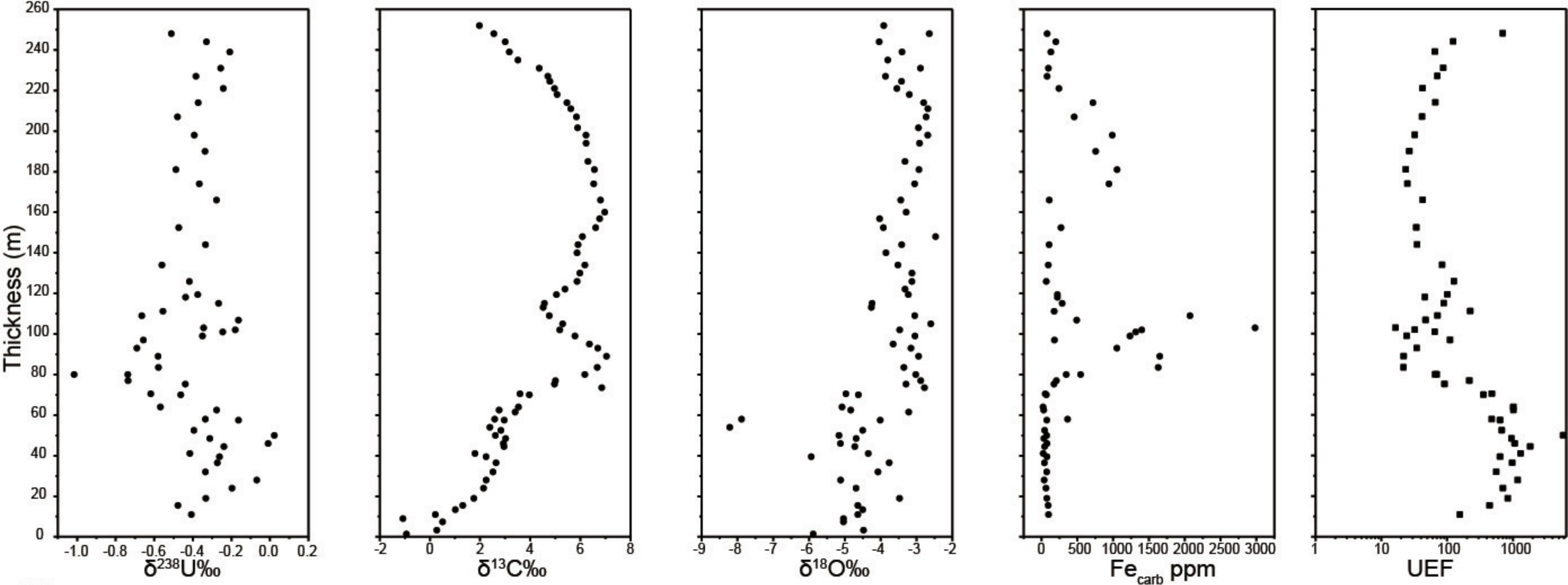
Thickness (m)
δ238U‰
δ13C‰
δ18O‰
Fecarb ppm
UEF
Pcarb ppm
Alcarb ppm
Thcarb ppm

**Table DR1.** Description, depositional environment and oxygenation interpretations of Joana Limestone and Limestone X facies at Pahranaghat Range section, southern Nevada, USA.

| Facies | Lime mudstone | Lime mudstone-wackestone | Skeletal wackestone | Packstone |
|---|---|---|---|---|
| **Lithology** | Dark gray, lime mudstone | Dark gray, skeletal lime mudstone-wackestone | Dark gray, skeletal wackestone, sparse chert nodules/layers | Medium to light gray, crinoidal packstone |
| **Sedimentary structures** | Medium to thin bedded, suspension laminations, graded beds | Medium to thin bedded, nodular bedding, graded beds, lenticular beds, sparse suspension laminations | Medium to thin bedded, nodular bedding, graded beds | Medium- to thick-bedded, nodular bedding, rare preserved cross bedding |
| **Skeletal/trace fossils** | Sparse crinoids, brachiopods, tabulate corals; sparse bioturbation including *Zoophycus* and *Chondrites* | Whole or broken crinoids, brachiopods, rugose corals, bioturbation, including sparse *Zoophycus* | Whole or broken rugose corals, brachiopods, crinoids, gastropods bioturbation | Whole or broken crinoids, brachiopods, rugose corals, abundant bioturbation |
| **Depositional environment and oxygenation interpretations** | Poorly to moderately oxygenated, offshore to lower shoreface, outer ramp | Moderately oxygenated, lower shoreface, middle to outer ramp | Moderately oxygenated, lower shoreface, middle ramp | Well oxygenated, upper shoreface, Inner ramp |

**Table DR2.** Parameters used in dynamic U modeling.

| Parameter | Value | Reference |
|---|---|---|
| $\delta^{238}U_{river}$ | -0.29‰ | |
| $J_{river}$ | $4.20 \times 10^{16}$ nmol/yr | Morford and Emerson, 1999 |
| $k_{oxic}$ | 28 nmol/m$^2$·yr·nMU | Dunk et al., 2002 |
| $k_{anox}$ | 629 nmol/m$^2$·yr·nMU | Zheng et al., 2000, 2002; McManus et al., 2006 |
| $\Delta_{oxic}$ | 0‰ | Tissot and Dauphas, 2015; Anderson et al., 2017 |
| $\Delta_{anox}$ | 0.65‰ | Tissot and Dauphas, 2015; Anderson et al., 2017 |
| Ao | $3.62 \times 10^{14}$ m$^2$ | Lutgens, Frederick. Essentials of Geology. New York: MacMillan, 1992: 269 p. |
| Vo | $1.34 \times 10^{21}$ L | "The World Ocean." The Columbia Encyclopedia. CD-ROM. 2007, 6th Ed. New York: Columbia University Press |
| $\delta^{238}U_{initial}$ | -0.68 | First value of $\delta^{238}$U curve |
| U conc $_{initial}$ | $1.74 \times 10^{-9}$ | Calculated from steady state |
| $F_{anox\ initial}$ | 6% | Calculated from steady state |

**Table DR3.** Parameters used in carbon burial modeling.

| Parameter | Value | Reference |
|---|---|---|
| $F_w$ | $56000 \times 10^{12}$ mol/ky | Kump and Arthur, 1999 |
| $F_{bcarb}$ | $40000 \times 10^{12}$ mol/ky | Kump and Arthur, 1999 |
| $F_{borg}$ | $10000 \times 10^{12}$ mol/ky | Kump and Arthur, 1999 |
| $\delta^{13}C_w$ | -3.97‰ | Calculated from steady state |
| $\Delta_{org}$ | -25‰ | Kump and Arthur, 1999 |
| $\Delta_{carb}$ | 0‰ | Calculated from steady state |
| $\delta^{13}C_{initial}$ | 0.49‰ | From measurements |
| Anoxic OC burial | 307.29 mol/m$^2$/ky | Berner, 1982 |
| Oxic OC burial | 15.16 mol/m$^2$/ky | Calculated from Early Mississippian background $f_{anox}$ |
| Background $f_{anox}$ | 4% | Average of pre-and post-Tournaisian OAE $\delta^{238}U$ values |

| Sample # | meters m | $\delta^{13}C$ ‰ | $\delta^{18}O$ ‰ | $\delta^{238}U$ ‰ | 2sd | Mg (ppm) | Al (ppm) | P (ppm) | Ca (ppm) | V (ppm) | Mn (ppm) | Fe (ppm) | Sr (ppm) | Mo (ppm) | Re (ppm) | Th (ppm) | U (ppm) | lithology |
|---|---|---|---|---|---|---|---|---|---|---|---|---|---|---|---|---|---|---|
| PR1.4 | 1.4 | -0.94 | -5.89 | | | | | | | | | | | | | | | WK |
| PR3.3 | 3.3 | | | | | | | | | | | | | | | | | MST |
| PR7.4 | 7.4 | 0.51 | -5.04 | | | | | | | | | | | | | | | WK |
| PR9 | 9 | -1.08 | -5.04 | | | | | | | | | | | | | | | WK |
| PR11 | 11 | 0.22 | -4.64 | -0.41 | 0.16 | 3990 | 58.7 | 25.8 | 373840 | 0.62 | 21.4 | 97.6 | 374.9 | 0.03 | 0.00020 | 0.07 | 0.28 | WK |
| PR13.4 | 13.4 | | | | | | | | | | | | | | | | | PK |
| PR15.5 | 15.5 | 1.31 | -4.64 | -0.48 | 0.02 | 2408 | 23.8 | 22.4 | 364809 | 1.00 | 12.5 | 93.1 | 301.5 | 0.07 | 0.00013 | 0.02 | 0.33 | PK |
| PR17.5 | 17.5 | | | | | | | | | | | | | | | | | PK |
| PR19 | 19 | 1.75 | -3.48 | -0.33 | 0.16 | 2895 | 22.3 | 23.3 | 371872 | 1.48 | 11.4 | 74.1 | 323.5 | 0.06 | 0.00020 | 0.03 | 0.58 | PK |
| PR21.2 | 21.2 | | | | | | | | | | | | | | | | | WK |
| PR24 | 24 | 2.14 | -4.69 | -0.20 | 0.06 | 3077 | 20.5 | 17.2 | 373841 | 2.09 | 12.3 | 61.7 | 338.4 | 0.06 | 0.00015 | 0.06 | 0.45 | PK |
| PR26 | 26 | | | | | | | | | | | | | | | | | WK |
| PR28 | 28 | 2.24 | -5.12 | -0.07 | 0.08 | 2346 | 28.1 | 19.8 | 376319 | 4.14 | 14.7 | 37.4 | 354.3 | 0.04 | 0.00036 | 0.05 | 1.03 | WK |
| PR30.6 | 30.6 | | | | | | | | | | | | | | | | | WK |
| PR32 | 32 | 2.52 | -4.08 | -0.33 | 0.04 | 3204 | 36.5 | 20.5 | 374360 | 2.07 | 17.3 | 72.3 | 339.1 | 0.04 | 0.00020 | 0.06 | 0.63 | WK |
| PR34.3 | 34.3 | | | | | | | | | | | | | | | | | PK |
| PR36.5 | 36.5 | 2.64 | -3.77 | -0.27 | 0.05 | 2947 | 19.6 | 30.9 | 376042 | 2.54 | 20.4 | 40.5 | 406.1 | 0.06 | 0.00034 | 0.01 | 0.59 | PK |
| PR37.8 | 37.8 | | | | | | | | | | | | | | | | | WK-PK |
| PR39.5 | 39.5 | 2.24 | -5.94 | | | 2760 | 41.9 | 27.7 | 374310 | 2.63 | 15.0 | 75.5 | 331.2 | 0.03 | 0.00019 | 0.07 | 0.83 | WK-PK |
| PR41.1 | 41.1 | | | | | | | | | | | | | | | | | WK-PK |
| PRX0.6 | 41.1 | | | -0.42 | 0.02 | 2985 | 17.6 | 84.6 | 379558 | 3.41 | 72.9 | 23.6 | 768.8 | 0.01 | 0.00013 | 0.02 | 0.71 | WK-PK |
| PR42 | 42 | | | | | | | | | | | | | | | | | WK-PK |
| PR42.5 | 42.5 | | | | | | | | | | | | | | | | | WK-PK |
| PRX2 | 42.5 | | | | | | | | | | | | | | | | | WK-PK |
| PR44 | 44 | | | | | | | | | | | | | | | | | WK-PK |
| PR44.5 | 44.5 | | | | | | | | | | | | | | | | | WK-PK |
| PRX4 | 44.5 | 2.96 | -4.72 | -0.24 | 0.02 | 1799 | 9.5 | 71.6 | 375807 | 2.50 | 65.8 | 43.1 | 394.5 | 0.01 | 0.00006 | 0.04 | 0.54 | WK-PK |
| PR46 | 46 | 2.93 | -5.13 | -0.01 | 0.04 | 2221 | 24.2 | 30.5 | 373191 | 3.33 | 15.9 | 76.7 | 323.9 | 0.05 | 0.00031 | 0.05 | 0.80 | WK-PK |
| PR46.5 | 46.5 | | | | | | | | | | | | | | | | | WK-PK |
| PRX6 | 46.5 | | | | | | | | | | | | | | | | | WK-PK |
| PR48 | 48 | | | | | | | | | | | | | | | | | WK-PK |
| PR48.5 | 48.5 | | | | | | | | | | | | | | | | | WK-PK |
| PRX8 | 48.5 | 3.02 | -4.69 | -0.31 | 0.05 | 2242 | 9.4 | 74.7 | 381914 | 1.69 | 72.5 | 33.0 | 308.3 | 0.02 | 0.00009 | 0.03 | 0.28 | WK-PK |
| PR50 | 50 | 2.61 | -5.17 | | | 2548 | 13.5 | 30.9 | 379982 | 11.40 | 20.9 | 72.4 | 344.4 | 0.04 | 0.00041 | 0.03 | 2.44 | WK-PK |

| | | | | | | | | | | | | | | | | | | |
|---|---|---|---|---|---|---|---|---|---|---|---|---|---|---|---|---|---|---|
| PR50.5 | 50.5 | | | | | | | | | | | | | | | | | WK-PK |
| PRX10 | 50.5 | | | | | | | | | | | | | | | | | WK-PK |
| PR51.5 | 51.5 | | | | | | | | | | | | | | | | | WK-PK |
| PR52.5 | 52.5 | | | | | | | | | | | | | | | | | WK-PK |
| PRX12 | 52.5 | 2.83 | -4.50 | -0.39 | 0.09 | 2252 | 23.8 | 115.3 | 373867 | 1.77 | 133.8 | 43.6 | 287.2 | 0.02 | 0.00011 | 0.05 | 0.50 | WK-PK |
| PR54 | 54 | 2.39 | -8.21 | | | | | | | | | | | | | | | WK-PK |
| PR55 | 55 | | | | | | | | | | | | | | | | | WK-PK |
| PRX14.5 | 55 | | | | | | | | | | | | | | | | | WK-PK |
| PR55.5 | 55.5 | | | | | | | | | | | | | | | | | WK-PK |
| PR57.5 | 57.5 | | | | | | | | | | | | | | | | | WK |
| PRX17 | 57.5 | 2.96 | -4.01 | -0.16 | 0.04 | 3931 | 31.8 | 110.0 | 363609 | 2.49 | 112.6 | 72.8 | 395.7 | 0.02 | 0.00009 | 0.07 | 0.63 | WK |
| PR58 | 58 | 2.58 | -7.89 | -0.34 | 0.03 | 2344 | 47.3 | 168.6 | 293767 | 2.57 | 29.0 | 364.2 | 466.0 | 0.03 | 0.00014 | 0.08 | 0.70 | WK |
| PR59.4 | 59.4 | | | | | | | | | | | | | | | | | WK |
| PRX18.9 | 59.4 | | | | | | | | | | | | | | | | | WK |
| PR60 | 60 | | | | | | | | | | | | | | | | | WK |
| PR61.5 | 61.5 | | | | | | | | | | | | | | | | | WK |
| PRX21 | 61.5 | 3.40 | -3.22 | | | | | | | | | | | | | | | WK |
| PR62.5 | 62.5 | 2.76 | -4.84 | -0.28 | 0.08 | 2627 | 27.0 | 169.4 | 382455 | 3.13 | 53.1 | 30.7 | 611.9 | 0.02 | 0.00012 | 0.03 | 0.85 | WK |
| PR64 | 64 | | | | | | | | | | | | | | | | | WK |
| PR64 | 64 | | | | | | | | | | | | | | | | | WK-PK |
| PRX23.5 | 64 | 3.53 | -5.08 | -0.58 | 0.01 | 2451 | 12.0 | 120.1 | 366252 | 2.46 | 67.3 | 21.9 | 298.4 | 0.01 | 0.00002 | 0.02 | 0.38 | WK-PK |
| PR66 | 66 | | | | | | | | | | | | | | | | | WK |
| PR66 | 66 | | | | | | | | | | | | | | | | | WK-PK |
| PRX25.5 | 66 | | | | | | | | | | | | | | | | | WK-PK |
| PR68 | 68 | | | | | | | | | | | | | | | | | WK |
| PR68.5 | 68.5 | | | | | | | | | | | | | | | | | WK-PK |
| PRX28 | 68.5 | | | | | | | | | | | | | | | | | WK-PK |
| PR70 | 70 | 3.96 | -4.62 | -0.46 | 0.05 | 2642 | 40.1 | 213.5 | 374947 | 2.06 | 53.2 | 66.9 | 489.0 | 0.01 | 0.00011 | 0.08 | 0.44 | WK |
| PR70.5 | 70.5 | | | | | | | | | | | | | | | | | PK-GST |
| PRX30 | 70.5 | 3.59 | -4.97 | -0.62 | 0.03 | 2201 | 23.0 | 417.4 | 366929 | 1.48 | 98.0 | 52.2 | 367.8 | 0.02 | 0.00009 | 0.05 | 0.34 | PK-GST |
| PR72 | 72 | | | | | | | | | | | | | | | | | PK |
| PR72 | 72 | | | | | | | | | | | | | | | | | PK |
| PRX31.5 | 72 | | | | | | | | | | | | | | | | | PK |
| PR73.5 | 73.5 | | | | | | | | | | | | | | | | | PK |
| PR73.5 | 73.5 | | | | | | | | | | | | | | | | | MST-WK |
| PRX33 | 73.5 | 6.85 | -2.78 | | | | | | | | | | | | | | | MST-WK |
| PR75.3 | 75.3 | 4.97 | -3.29 | -0.44 | 0.09 | 3189 | 89.8 | 67.0 | 380409 | 1.24 | 44.4 | 174.3 | 559.4 | 0.02 | 0.00012 | 0.13 | 0.25 | MST-WK |

| | | | | | | | | | | | | | | | | | | |
|---|---|---|---|---|---|---|---|---|---|---|---|---|---|---|---|---|---|---|
| PR75.5 | 75.5 | | | | | | | | | | | | | | | | | MST-WK |
| PRX35 | 75.5 | | | | | | | | | | | | | | | | | MST-WK |
| PR77 | 77 | | | | | | | | | | | | | | | | | WK-PK |
| PR77 | 77 | | | | | | | | | | | | | | | | | WK-PK |
| PRX36.5 | 77 | 5.01 | -2.88 | -0.74 | 0.06 | 4025 | 47.7 | 64.5 | 377872 | 0.95 | 37.5 | 207.6 | 397.5 | 0.02 | 0.00037 | 0.10 | 0.32 | WK-PK |
| PR78 | 78 | | | | | | | | | | | | | | | | | PK |
| PR80 | 80 | 6.18 | -3.02 | -0.74 | 0.36 | 3365 | 106.0 | 145.5 | 326086 | 6.64 | 70.2 | 545.7 | 717.6 | 0.02 | 0.00085 | 0.10 | 0.23 | MST-WK |
| PR80 (dup.) | 80 | | | -1.02 | 0.15 | 3173 | 93.6 | 151.4 | 294545 | 6.36 | 67.8 | 345.0 | 680.8 | 0.01 | 0.00056 | 0.11 | 0.19 | MST-WK |
| PR81.8 | 81.8 | | | | | | | | | | | | | | | | | MST-WK |
| PR83.5 | 83.5 | 6.68 | -3.35 | -0.58 | 0.16 | 4953 | 183.9 | 70.0 | 355654 | 2.14 | 63.3 | 1629.6 | 820.6 | 0.03 | 0.00072 | 0.35 | 0.12 | MST |
| PR85.5 | 85.5 | | | | | | | | | | | | | | | | | MST |
| PR87 | 87 | | | | | | | | | | | | | | | | | MST |
| PR89 | 89 | 7.04 | -2.94 | -0.58 | 0.09 | 4978 | 186.1 | 71.2 | 358668 | 2.14 | 63.8 | 1650.2 | 824.0 | 0.04 | 0.00068 | 0.36 | 0.13 | MST |
| PR91 | 91 | | | | | | | | | | | | | | | | | MST |
| PR93 | 93 | 6.69 | -3.16 | -0.69 | 0.11 | 3790 | 180.5 | 33.0 | 359207 | 2.18 | 38.8 | 1052.0 | 840.6 | 0.04 | 0.00096 | 0.26 | 0.19 | MST |
| PR95 | 95 | 6.36 | -3.65 | | | | | | | | | | | | | | | MST |
| PR97 | 97 | | | -0.66 | 0.14 | 4205 | 62.1 | 26.5 | 322306 | 3.34 | 31.5 | 180.9 | 503.7 | 0.02 | 0.00024 | 0.11 | 0.21 | MST-WK |
| PR99 | 99 | 5.79 | -3.04 | -0.35 | 0.06 | 15758 | 307.9 | 30.9 | 317164 | 3.00 | 54.2 | 1234.8 | 509.6 | 0.06 | 0.00049 | 0.31 | 0.23 | MST |
| PR101 | 101 | | | -0.24 | 0.01 | 6529 | 172.6 | 38.8 | 256376 | 4.82 | 51.5 | 1315.0 | 532.7 | 0.08 | 0.00363 | 0.31 | 0.35 | MST |
| PR102 | 102 | 5.18 | -3.47 | -0.18 | 0.05 | 4430 | 295.9 | 38.8 | 313030 | 4.65 | 52.4 | 1398.8 | 729.4 | 0.05 | 0.00210 | 0.39 | 0.30 | MST-WK |
| PR103 | 103 | | | -0.34 | 0.00 | 6946 | 413.4 | 36.4 | 245866 | 4.35 | 64.7 | 2981.3 | 582.2 | 0.10 | 0.00371 | 0.64 | 0.21 | MST-WK |
| PR105 | 105 | 5.30 | -2.60 | | | | | | | | | | | | | | | MST-WK |
| PR106.8 | 106.8 | | | -0.16 | 0.09 | 3113 | 205.3 | 38.4 | 309129 | 4.63 | 60.3 | 491.0 | 723.2 | 0.01 | 0.00015 | 0.34 | 0.30 | MST |
| PR109 | 109 | 4.76 | -3.05 | -0.66 | 0.02 | 4116 | 178.0 | 41.3 | 325811 | 10.76 | 61.1 | 2073.0 | 632.9 | 0.17 | 0.00193 | 0.18 | 0.39 | MST-WK |
| PR111.2 | 111.2 | | | | | 4252 | 56.6 | 36.7 | 329777 | 4.66 | 34.5 | 176.6 | 1094.9 | 0.02 | 0.00060 | 0.09 | 0.39 | MST-WK |
| PR113.1 | 113.1 | 4.52 | -4.26 | | | | | | | | | | | | | | | MST-WK |
| PR115.1 | 115.1 | 4.57 | -4.24 | | | 2455 | 145.2 | 36.3 | 270901 | 5.18 | 36.9 | 288.8 | 546.5 | 0.01 | 0.00022 | 0.26 | 0.40 | MST-WK |
| PR118.1 | 118.1 | | | | | 3061 | 230.5 | 44.2 | 315371 | 3.50 | 38.1 | 221.6 | 540.8 | 0.00 | 0.00005 | 0.46 | 0.33 | MST |
| PR119.4 | 119.4 | 5.05 | -3.23 | -0.37 | 0.16 | 3757 | 104.8 | 50.9 | 363844 | 2.15 | 35.7 | 222.0 | 518.9 | 0.01 | 0.00017 | 0.27 | 0.33 | MST-WK |
| PR122.1 | 122.1 | 5.39 | -3.32 | | | | | | | | | | | | | | | MST-WK |
| PR124 | 124 | | | | | | | | | | | | | | | | | MST-WK |
| PR125.9 | 125.9 | 5.87 | -3.13 | -0.42 | 0.20 | 3438 | 55.3 | 69.9 | 369460 | 1.06 | 21.8 | 65.9 | 816.0 | 0.02 | 0.00014 | 0.09 | 0.22 | MST-WK |
| PR128.2 | 128.2 | | | | | | | | | | | | | | | | | MST |
| PR130 | 130 | 5.98 | -3.13 | | | | | | | | | | | | | | | MST |
| PR132 | 132 | | | | | | | | | | | | | | | | | MST-WK |
| PR134 | 134 | 6.18 | -3.52 | -0.56 | 0.11 | 3256 | 63.5 | 61.3 | 374648 | 1.23 | 21.2 | 95.7 | 768.2 | 0.01 | 0.00013 | 0.12 | 0.16 | MST-WK |
| PR136 | 136 | | | | | | | | | | | | | | | | | MST-WK |

| | | | | | | | | | | | | | | | | | | |
|---|---|---|---|---|---|---|---|---|---|---|---|---|---|---|---|---|---|---|
| PR138 | 138 | | | | | | | | | | | | | | | | | MST-WK |
| PR140 | 140 | 5.87 | -3.86 | | | | | | | | | | | | | | | MST-WK |
| PR141.8 | 141.8 | | | | | | | | | | | | | | | | | MST-WK |
| PR144 | 144 | 5.91 | -3.42 | -0.33 | 0.08 | 7482 | 121.8 | 36.4 | 356083 | 1.81 | 25.7 | 105.6 | 682.3 | 0.02 | 0.00013 | 0.21 | 0.13 | MST-WK |
| PR146 | 146 | | | | | | | | | | | | | | | | | MST-WK |
| PR148 | 148 | 6.09 | -2.47 | | | | | | | | | | | | | | | WK-PK |
| PR149.9 | 149.9 | | | | | | | | | | | | | | | | | WK-PK |
| PR152.4 | 152.4 | 6.61 | -3.93 | | | 10852 | 156.7 | 104.1 | 348393 | 1.98 | 28.1 | 271.1 | 659.9 | 0.02 | 0.00032 | 0.18 | 0.16 | WK-PK |
| PR154 | 154 | | | | | | | | | | | | | | | | | WK-PK |
| PR156.8 | 156.8 | 6.77 | -4.03 | | | | | | | | | | | | | | | MST |
| PR158 | 158 | | | | | | | | | | | | | | | | | MST |
| PR160 | 160 | 6.97 | -3.29 | | | | | | | | | | | | | | | MST |
| PR162 | 162 | | | | | | | | | | | | | | | | | MST |
| PR164 | 164 | | | | | | | | | | | | | | | | | MST-WK |
| PR166 | 166 | 6.80 | -3.44 | -0.28 | 0.13 | 3417 | 106.9 | 47.9 | 373611 | 1.54 | 31.6 | 108.5 | 746.8 | 0.01 | 0.00007 | 0.19 | 0.14 | MST-WK |
| PR167.5 | 167.5 | | | | | | | | | | | | | | | | | MST-WK |
| PR172 | 172 | | | | | | | | | | | | | | | | | MST-WK |
| PR174 | 174 | 6.54 | -3.05 | -0.37 | 0.00 | 5887 | 186.5 | 44.5 | 359460 | 1.81 | 38.3 | 941.4 | 729.6 | 0.05 | 0.00042 | 0.30 | 0.14 | MST-WK |
| PR176.6 | 176.6 | | | | | | | | | | | | | | | | | MST-WK |
| PR179 | 179 | | | | | | | | | | | | | | | | | WK |
| PR181 | 181 | 6.56 | -2.93 | -0.49 | 0.18 | 5065 | 177.4 | 48.9 | 358588 | 1.78 | 43.6 | 1054.8 | 684.2 | 0.03 | 0.00045 | 0.33 | 0.13 | MST-WK |
| PR183 | 183 | | | | | | | | | | | | | | | | | MST-WK |
| PR185 | 185 | 6.31 | -3.32 | | | | | | | | | | | | | | | WK |
| PR187.2 | 187.2 | | | | | | | | | | | | | | | | | WK |
| PR190 | 190 | | | -0.34 | 0.14 | 3851 | 186.4 | 50.2 | 358961 | 1.62 | 43.7 | 756.2 | 598.1 | 0.02 | 0.00081 | 0.36 | 0.15 | WK |
| PR192 | 192 | | | | | | | | | | | | | | | | | WK |
| PR194 | 194 | 6.23 | -2.92 | | | | | | | | | | | | | | | MST-WK |
| PR196 | 196 | | | | | | | | | | | | | | | | | WK |
| PR198 | 198 | 6.23 | -2.69 | -0.39 | 0.05 | 6164 | 130.2 | 42.5 | 360032 | 1.52 | 33.2 | 988.1 | 621.1 | 0.04 | 0.00054 | 0.30 | 0.13 | WK |
| PR200 | 200 | | | | | | | | | | | | | | | | | WK |
| PR201.6 | 201.6 | 5.89 | -2.95 | | | | | | | | | | | | | | | WK |
| PR204 | 204 | | | | | | | | | | | | | | | | | WK |
| PR207 | 207 | 5.85 | -2.73 | -0.48 | 0.06 | 3607 | 107.4 | 42.6 | 367180 | 1.36 | 29.7 | 455.8 | 678.4 | 0.02 | 0.00026 | 0.20 | 0.14 | WK |
| PR209 | 209 | | | | | | | | | | | | | | | | | WK |
| PR211 | 211 | 5.62 | -2.68 | | | | | | | | | | | | | | | WK |
| PR213 | 213 | | | | | | | | | | | | | | | | | MST-WK |
| PR214 | 214 | 5.47 | -2.80 | -0.37 | 0.03 | 5261 | 113.5 | 38.8 | 369162 | 1.94 | 36.6 | 718.0 | 636.2 | 0.06 | 0.00066 | 0.25 | 0.23 | MST-WK |

| | | | | | | | | | | | | | | | | | |
|---|---|---|---|---|---|---|---|---|---|---|---|---|---|---|---|---|---|
| PR215 | 215 | | | | | | | | | | | | | | | | MST-WK |
| PR218 | 218 | 5.07 | -3.20 | | | | | | | | | | | | | | WK |
| PR221 | 221 | 4.97 | -3.55 | -0.24 | 0.08 | 2820 | 169.5 | 41.5 | 357065 | 2.44 | 44.7 | 243.1 | 497.7 | 0.02 | 0.00010 | 0.34 | 0.22 | WK |
| PR223 | 223 | | | | | | | | | | | | | | | | | MST-WK |
| PR224 | 224 | | | | | | | | | | | | | | | | | WK |
| PR227 | 227 | 4.71 | -3.87 | -0.38 | 0.02 | 3105 | 111.3 | 34.1 | 364260 | 1.72 | 26.8 | 77.3 | 577.2 | 0.01 | 0.00009 | 0.25 | 0.24 | WK |
| PR229 | 229 | | | | | | | | | | | | | | | | | MST-WK |
| PR231 | 231 | 4.36 | -2.89 | -0.26 | 0.08 | 4962 | 109.5 | 39.0 | 367061 | 1.94 | 30.8 | 96.2 | 539.8 | 0.02 | 0.00019 | 0.16 | 0.30 | MST-WK |
| PR233 | 233 | | | | | | | | | | | | | | | | | MST-WK |
| PR235 | 235 | 3.51 | -3.80 | | | | | | | | | | | | | | | MST-WK |
| PR237 | 237 | | | | | | | | | | | | | | | | | WK |
| PR239 | 239 | 3.17 | -3.41 | -0.21 | 0.00 | 3478 | 177.6 | 39.7 | 365844 | 2.37 | 46.7 | 130.7 | 475.3 | 0.01 | 0.00015 | 0.26 | 0.36 | WK |
| PR241 | 241 | | | | | | | | | | | | | | | | | MST |
| PR244 | 244 | 3.00 | -4.04 | -0.33 | 0.03 | 3053 | 105.1 | 30.6 | 349252 | 2.66 | 48.8 | 199.3 | 493.8 | 0.02 | 0.00027 | 0.30 | 0.40 | MST-WK |
| PR246 | 246 | | | | | | | | | | | | | | | | | MST-WK |
| PR248 | 248 | 2.55 | -2.65 | -0.51 | 0.00 | 3841 | 32.6 | 58.8 | 362155 | 3.36 | 76.8 | 77.9 | 326.9 | 0.04 | 0.00061 | 0.07 | 0.71 | MST-WK |
| PR250 | 250 | | | | | | | | | | | | | | | | | MST-WK |
| PR252 | 252 | 1.97 | -3.92 | | | | | | | | | | | | | | | MST-WK |
| PR19 | | | | -0.38 | 0.08 | 1242 | 7.3 | 7.6 | 156921 | 0.57 | 4.7 | 9.0 | 138.5 | 0.03 | 0.00006 | 0.00 | 0.18 | brachiopod |
| PRX23.5 | | | | -0.57 | | 3223 | 9.1 | 105.5 | 381614 | 1.46 | 71.6 | 17.0 | 317.5 | 0.01 | 0.00004 | 0.01 | 0.21 | crinoid |
| PR144 | | | | | | 1681 | 13.1 | 21.8 | 354776 | 0.12 | 10.9 | 8.0 | 312.0 | 0.01 | 0.00005 | 0.01 | 0.01 | rugose coral |
| PR214 | | | | -0.39 | 0.05 | 3592 | 9.7 | 18.4 | 348064 | 0.25 | 17.1 | 5.1 | 308.4 | 0.01 | 0.00007 | 0.00 | 0.03 | rugose coral |